Gain-scheduled EKF for Nano-satellite Attitude Determination System

M. D. Pham, K. S. Low, Senior Member of IEEE, S.T. Goh, Shoushun Chen

School of Electrical and Electronic Engineering

Nanyang Technological University, Singapore

***Abstract*–Extended Kalman filter (EKF) has been widely used for attitude determination in various satellite missions. However, it requires an extensive computational power which is not suitable for nano-satellite application. This paper proposes a gain-scheduled EKF (GSEKF) to reduce the computational requirement in nano-satellite attitude determination process. The proposed GSEKF eliminates the online recursive Kalman gain computation by analytically determines the Kalman gain based on the sensor parameters, such as the gyroscope noise variance, the quaternion variance, the observation matrix and the satellite rotational speed. Two GSEKF Kalman gains for two satellite operating modes are presented: the sun pointing and nadir pointing modes. The simulation and experimental results show that the proposed method has comparable attitude estimation accuracy to the conventional EKF. In addition, the proposed GSEKF reduces 86.29% and 89.45% of the computation load compared to the multiplicative EKF and Murrell's version.**

***Index terms*– Extended Kalman filter, satellite attitude determination, and nano-satellite.**

I. INTRODUCTION

The attitude determination system (ADS) is a critical subsystem for any satellite mission. In general, the ADS system consists of various sensors such as the three-axis gyroscope, three-axis magnetometer, sun sensors and star tracker. In addition, the differential Global Positioning System (GPS) carrier phase signal could be used to enhance the attitude determination accuracy for satellite that is equipped with low cost sensor, such as the coarse sun sensor [1].

The extended Kalman filter (EKF) using quaternion has been widely used in attitude estimation to prevent singularity of attitude measurements [2, 3]. It recursively integrates the satellite dynamic and sensor measurements to estimate the satellite's attitude in real-time. However the EKF using four-component quaternion is unable to maintain the quaternion norm constraint which leads to the estimation divergence. To enforce this constraint, the multiplicative EKF (MEKF) employs a three-component representation of attitude error and quaternion error multiplication to update the satellite quaternion [4-8].The Murrell version of MEKF further reduces the computational requirement by limiting a 3x1 observation vector to be taken for the updating process. Thus, only the 3×3 matrix inversion is required for each iterated update process[9]. The additive EKF (AEKF) estimates the quaternion by adding measured quaternion with quaternion error. To ensure unity constraint, the AEKF applies normalization to the measured quaternion [10, 11].

In addition, the sigma-point Kalman filter has been presented for attitude estimation in [12-14]. The algorithm has a higher and better accuracy consistency than the EKF, especially in the case of high initial estimation error [12, 14]. However, its computational requirement is higher than EKF. The matrix Kalman filter uses an optimal de-noising procedure and applied it into the time-varying noisy K-matrix to improve the optimal recursive quaternion estimation algorithm[15].Furthermore, the multiple model Kalman filter for attitude determination using gyroscope and star sensor has been presented in [16]. The square root quaternion cubature Kalman filtering uses a two-step projection method to maintain the quaternion normalization constraint along with the attitude estimation process [17]. The square root form inhibits an improved numerical stability by guarantee the covariance matrices always remain positive.

In recent years, there are growing numbers of nano-satellite projects from universities [18-24]. Nano-satellites are miniature satellites that are typically weighing in the range of 1-20kg. Several attitude determination methods have been employed in nano-satellite applications. As the EKF (and MEKF)involves the algebra of multi-dimension matrix (6x6 dimension matrixes) in real-time, a high performance microprocessor is required [19].This results in higher power consumption that may exceed the power constraint of a nano-satellite. To avoid on-board numerical computation, the satellite attitude is obtained from a look-up table of possible satellite orientation in [23].

The gain-scheduled method has been used in several applications such as the aircraft engine performance evaluation[25], power system state estimation[26], ship vessel navigation[27] and Unmanned Aerial Vehicles (UAV) [28]. The Kalman gain in [25] and [28] is approximates based on Riccati equation, which requires both sensor variances and state error covariance information. In addition, different scheduled Kalman gains are computed offline, and the corresponding Kalman gain is chosen by the algorithm based on the actual operating condition.

This paper proposes a gain-scheduled Extended Kalman Filter (GSEKF) for the nano-satellite attitude determination to reduce the EKF's computational cost. The two main contributions of this research are: the scheduled Kalman gain determination method and the elimination of online Kalman gain computation. The proposed GSEKF analytically determines the Kalman gain from the sensor parameters, such as the gyroscope noise variance, the measured quaternion variance, the observation matrix and the satellite rotational speed. In addition, the proposed Kalman gain is independent

of state error covariance. The Kalman gains for sun pointing mode and nadir pointing mode are computed offline. Then, the GSEKF uses these Kalman gains for updating process, instead of calculates its gain iteratively in every time step as in the conventional EKF. The GSEKF also employs multiplicative quaternion update in MEKF [4-8].Simulation and experimental study have been conducted to compare the accuracy between the proposed GSEKF and MEKF. In addition, the computational costs of GSEKF, MEKF and conventional EKF have been analysed.

The outline of this paper is as follows. Section II introduces the attitude determination system configuration. Section III describes the sensor noise characterization. In addition, sensor calibration procedures are presented. Section IV presents the proposed scheduled Kalman gain determination method for two satellite operating modes. Finally, section V presents the simulation and experimental results.

II. ATTITUDE DETERMINATION SYSTEM

The ADS in a nano-satellite is presented in Fig.1. The attitude sensors comprise of a sun sensor, a three-axis magnetometer, and a three-axis gyroscope. For the nano-satellite named VELOX-I that we have developed, there are two types of sun sensors: Position sensitive device (PSD) based fine sun sensor, and coarse sun sensor. The PSD sun sensor provides three axis sun vectors. The coarse sun sensor is a photodiode which provides two-axis information. The three-axis magnetometer measures the earth magnetic field direction in the satellite body frame [29, 30]. The three-axis gyroscope measures the satellite rotational speed and is used to propagate the satellite attitude over time. These sensors are interfaced with a microcontroller which stores the attitude determination algorithm. The system also includes the orbit propagator, the earth magnetic field model, and the sun vector model.

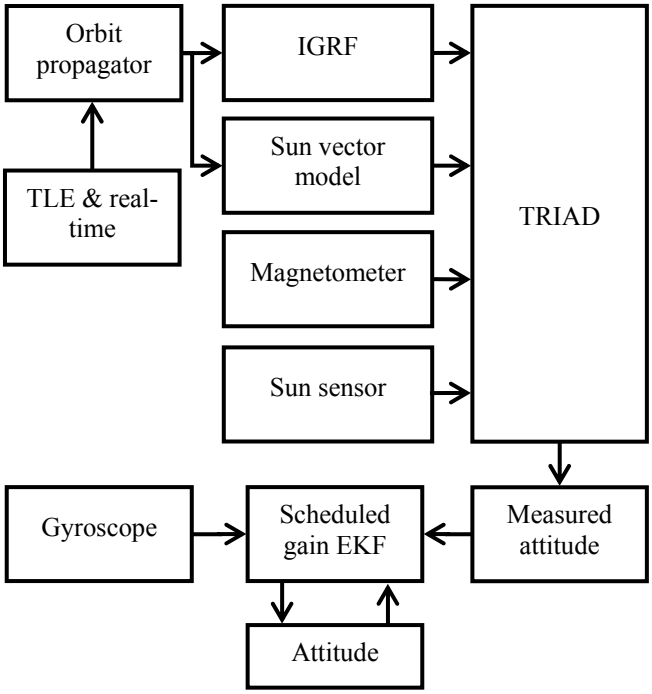

Fig.1: Satellite attitude determination system

The TRIAD method [31] is used to calculate the measured quaternion or measurement vector based on sun sensor and magnetometer measurements. The measurement matrix becomes an identity matrix with the measurement vector is a 3x1 quaternion vector, so the SGEKF formulation could be further simplified. The proposed gain-scheduled extended Kalman filter combines the gyroscope reading and the measured attitude to produce the optimal satellite attitude. The orbit propagator, the earth magnetic field, and the sun vector model are used to calculate the satellite position, earth magnetic field and the sun vector in the earth centre inertial (ECI) frame. First, the orbit propagator model routinely computes the satellite's position and velocity using the orbital parameters. These parameters are uplinked from the ground station. It is implemented based on the Kepler model [32]. Second, the International Geomagnetic Reference Field (IGRF-11th) has been implemented to estimate the magnetic field reference[33]. The IGRF model outputs three axes magnetic field vectors. The sun vector model calculates the sun illumination vector in the earth centre inertial frame. The gyroscope drift causes the attitude propagation error over time. Hence, the gain-scheduled extended Kalman filter is proposed to compensate for this error. The GSEKF state vector includes quaternion vector, q_e, and the gyroscope bias ω_{bias}.

III. ATTITUDE SENSOR CHARACTERIZATION

In this section, the noise variances of the attitude sensors are characterized. These noise variances are then used to determine the Kalman gain in section IV. The process noise covariance, **Q,** and the measurement noise covariance, **R,** are used to determine the Kalman gain in the GSEKF. The matrix **Q** is formulated from the gyroscope noise variance. From Fig.1, the measurement vector is the measured quaternion which is calculated by the TRIAD method. The matrix **R** is formulated from the magnetometer noise variance and the sun sensor noise variance.

A- Gyroscope noise characterization

The gyroscope signal contains the true angular rate, $\boldsymbol{\omega}$, in three axes, the constant bias, $\boldsymbol{\omega}_{bias}$, and the noise components, $\boldsymbol{\eta}_n$ and $\boldsymbol{\eta}_{bias}$ [34].

$$\tilde{\boldsymbol{\omega}}_{measured} = \boldsymbol{\omega} + \boldsymbol{\omega}_{bias} + \boldsymbol{\eta}_{bias} + \boldsymbol{\eta}_n \quad (1)$$

where the overhead "tilde" represents the measured angular rate. The constant gyroscope bias, $\boldsymbol{\omega}_{bias}$, is its average output when it is not undergoing any rotation. The constant bias is determined through the calibration procedure and compensated in the gyroscope reading. The term $\boldsymbol{\eta}_{bias}$ represents a time-varying component of the bias which is given as [34]:

$$\dot{\boldsymbol{\eta}}_{bias}(t) = -\frac{1}{\tau}\boldsymbol{\eta}_{bias}(t) + \mathbf{w}_{bias} \quad (2)$$

where $\mathbf{w}_{bias}$ is the driving process noise, τ denotes correlation time, and the term $\boldsymbol{\eta}_{bias}$ can be also assumed as an exponentially correlated Gaussian random process $E\left\{\boldsymbol{\eta}_{bias}\boldsymbol{\eta}_{bias}^T\right\} = \sigma_{bias}^2$. The term $\boldsymbol{\eta}_\eta$ is sampling noise which

can be modelled as white noise. Its standard deviation is σ_n.

B- Measurement noise characterization

The measured satellite attitude is calculated based on the ECI sun vector $\mathbf{S}^{ECI}$, sun sensor output $\mathbf{S}^{B}$, the ECI magnetic field $\mathbf{B}^{ECI}$ and the magnetometer output $\mathbf{B}^{B}$. The TRIAD method is based on constructing two triads of orthogonal unit vectors[35]. The two triads are the components of the same reference frame expressed in the body and inertial frame. The first base vector is constructed as:

$$\mathbf{t}_1^{B} = \mathbf{S}^{B} \tag{3}$$

$$\mathbf{t}_1^{ECI} = \mathbf{S}^{ECI} \tag{4}$$

The second base vector is constructed as a unit vector in the direction perpendicular to the two observations.

$$\mathbf{t}_2^{B} = \frac{\mathbf{S}^{B} \times \mathbf{B}^{B}}{\left|\mathbf{S}^{B} \times \mathbf{B}^{B}\right|} \tag{5}$$

$$\mathbf{t}_2^{ECI} = \frac{\mathbf{S}^{ECI} \times \mathbf{B}^{ECI}}{\left|\mathbf{S}^{ECI} \times \mathbf{B}^{ECI}\right|} \tag{6}$$

The third base is chosen to complete the orthogonal triad:

$$\mathbf{t}_3^{B} = \mathbf{t}_1^{B} \times \mathbf{t}_2^{B} \tag{7}$$

$$\mathbf{t}_3^{ECI} = \mathbf{t}_1^{ECI} \times \mathbf{t}_2^{ECI} \tag{8}$$

The attitude matrix can be obtained from:

$$\mathbf{A}_{ECI}^{B} = \mathbf{A}_{T}^{B}\mathbf{A}_{ECI}^{T} = [\mathbf{t}_1^{B}\mathbf{t}_2^{B}\mathbf{t}_3^{B}][\mathbf{t}_1^{ECI}\mathbf{t}_2^{ECI}\mathbf{t}_3^{ECI}]^{T} \tag{9}$$

Finally, the satellite attitude matrix $\mathbf{A}_{ECI}^{B}$ is converted into the quaternion representation. The measured attitude noise variance can be determined using the noise variance of $\mathbf{s}^{ECI}$, $\mathbf{s}^{B}$, $\mathbf{b}^{ECI}$, and $\mathbf{b}^{B}$. Assuming that there is no cross-correlation between each noise variance element, the variance analysis of the TRIAD algorithm is presented from (10) to(16).

$$\mathrm{var}\left(\mathbf{t}_1^{B}\right) = \mathrm{var}\left(\mathbf{s}^{B}\right) = \begin{bmatrix} \sigma^2_{\mathbf{s}_x^B} & \sigma^2_{\mathbf{s}_y^B} & \sigma^2_{\mathbf{s}_z^B} \end{bmatrix}^{T} \tag{10}$$

$$\mathrm{var}\left(\mathbf{t}_1^{ECI}\right) = \mathrm{var}\left(\mathbf{s}^{ECI}\right) = \begin{bmatrix} \sigma^2_{\mathbf{s}_x^{ECI}} & \sigma^2_{\mathbf{s}_y^{ECI}} & \sigma^2_{\mathbf{s}_z^{ECI}} \end{bmatrix}^{T} \tag{11}$$

$$\mathrm{var}\left(\mathbf{t}_2^{B}\right) = \mathrm{var}\left(\mathbf{s}^{B} \times \mathbf{s}^{B}\right) = \mathrm{var}\left(\mathbf{s}^{B}\right) \times \mathrm{var}\left(\mathbf{b}^{B}\right) \tag{12}$$

$$\mathrm{var}\left(\mathbf{t}_2^{ECI}\right) = \mathrm{var}\left(\mathbf{s}^{ECI} \times \mathbf{b}^{ECI}\right) = \mathrm{var}\left(\mathbf{s}^{ECI}\right) \times \mathrm{var}\left(\mathbf{b}^{ECI}\right) \tag{13}$$

$$\mathrm{var}\left(\mathbf{t}_3^{B}\right) = \mathrm{var}\left(\mathbf{t}_1^{B} \times \mathbf{t}_2^{B}\right) = \mathrm{var}\left(\mathbf{t}_1^{B}\right) \times \mathrm{var}\left(\mathbf{t}_2^{B}\right) \tag{14}$$

$$\mathrm{var}\left(\mathbf{t}_3^{ECI}\right) = \mathrm{var}\left(\mathbf{t}_1^{ECI} \times \mathbf{t}_2^{ECI}\right) = \mathrm{var}\left(\mathbf{t}_1^{ECI}\right) \times \mathrm{var}\left(\mathbf{t}_2^{ECI}\right) \tag{15}$$

The noise variance of the rotational matrix **A** can be determined as the vector product using the results from(10) to (15) as

$$\mathrm{var}\left(\mathbf{A}_{ECI}^{B}\right) = \mathrm{var}\left([\mathbf{t}_1^{B} \quad \mathbf{t}_1^{B} \quad \mathbf{t}_1^{B}][\mathbf{t}_1^{ECI} \quad \mathbf{t}_2^{ECI} \quad \mathbf{t}_3^{ECI}]^{T}\right) \tag{16}$$

Finally, the noise variance of the measured attitude is given as follows:

$$\mathrm{var}(\mathbf{q}) = \begin{bmatrix} \sigma^2_{q_1} & \sigma^2_{q_2} & \sigma^2_{q_3} & \sigma^2_{q_4} \end{bmatrix}^{T} \tag{17}$$

where, the subscript "q_1", "q_2", "q_3" and "q_4" represent the four elements of quaternion such that

$$\mathbf{q} = \begin{bmatrix} q_1 & q_2 & q_3 & q_4 \end{bmatrix}^{T} = \begin{bmatrix} q_1 & \mathbf{q}_e^{T} \end{bmatrix}^{T} \tag{18}$$

with q_1 is the scalar element of quaternion and $\mathbf{q_e}$ is the vector element of quaternion.

IV. GAIN SCHEDULED EXTENDED KALMAN FILTER

A- Extended Kalman filter for attitude determination

The dynamics of the satellite can be represented in a state space model [2-4] as follows

$$\mathbf{x}_k = \mathbf{\Phi}\mathbf{x}_{k-1} + \mathbf{G}\mathbf{w}_{k-1} \tag{19}$$

$$\mathbf{y}_k = \mathbf{H}\mathbf{x}_k + \mathbf{v}_k \tag{20}$$

where the state vector, **x**, contains the vector element of quaternion, $\mathbf{q}_e$ defined in (18), and the gyroscope bias $\left(\boldsymbol{\omega}_{bias} + \boldsymbol{\eta}_{bias}\right)$:

$$\mathbf{x} = \begin{bmatrix} \mathbf{q}_e^{T} & \left(\boldsymbol{\omega}_{bias} + \boldsymbol{\eta}_{bias}\right)^{T} \end{bmatrix}^{T} \tag{21}$$

Moreover, $\mathbf{x}_k$ and $\mathbf{x}_{k-1}$ denote the current and previous state vectors. The measurement vector is defined as

$$\mathbf{y} = \mathbf{q}_e \tag{22}$$

The matrix **H** in (20)is known as the observation matrix. The state transition matrix, **Φ**, propagates the state vector in each time step Δt. In practice, the time step is chosen as small as possible (i.e. 1ms to 10ms) to reduce the gyroscope drift effect ($\boldsymbol{\omega}_{bias} + \boldsymbol{\eta}_{bias} + \boldsymbol{\eta}_{n}$). The matrix **G** maps the process noise into the state vector and can be determined as follow [4, 5]

$$\mathbf{\Phi} = \mathbf{I}_{6?} + \begin{bmatrix} -\frac{1}{2}\mathrm{skew}(\boldsymbol{\omega}) & -\frac{1}{2}\mathbf{I}_{3\times3} \\ \mathbf{0}_{3\times3} & \mathbf{0}_{3\times3} \end{bmatrix}\Delta t \tag{23}$$

$$\mathbf{G} = \begin{bmatrix} -\frac{1}{2}\mathbf{I}_{3\times3} & \mathbf{0}_{3\times3} \\ \mathbf{0}_{3\times3} & -\frac{1}{2}\mathbf{I}_{3\times3} \end{bmatrix} \tag{24}$$

$$\mathbf{H} = \begin{bmatrix} \mathbf{I}_{3\times3} & \mathbf{0}_{3\times3} \end{bmatrix} \tag{25}$$

The process noise covariance, **Q**, can be constructed based on the gyroscope noise variance, $\boldsymbol{\sigma}^2_n$, as.

$$\mathbf{Q} = \mathrm{diag}\begin{bmatrix} \sigma^2_{n,x} & \sigma^2_{n,y} & \sigma^2_{n,z} & \sigma^2_{bias,x} & \sigma^2_{bias,y} & \sigma^2_{bias,z} \end{bmatrix} \tag{26}$$

Where "diag[]" denotes the diagonal matrix. The measurement noise covariance, **R**, can be constructed based on the quaternion noise variance.$\boldsymbol{\sigma}^2_q$, obtained from (17) as

$$\mathbf{R} = \mathrm{diag}\begin{bmatrix} \sigma^2_{q_2} & \sigma^2_{q_3} & \sigma^2_{q_4} \end{bmatrix} \tag{27}$$

The EKF operates recursively on streams of noisy attitude measurements to calculate statistically the optimal system state. The state error covariance, **P**, and the Kalman gain, **K**, are computed for every time step as follows:

$$\mathbf{P}_k^{-} = \mathbf{\Phi}_k \cdot \mathbf{P}_{k-1}^{+} \cdot \mathbf{\Phi}_k^{T} + \mathbf{Q} \tag{28}$$

$$\mathbf{K}_k = \mathbf{P}_k^{-} \cdot \mathbf{H}^{T} \cdot \left(\mathbf{H} \cdot \mathbf{P}_k^{-} \cdot \mathbf{H}^{T} + \mathbf{R}\right)^{-1} \tag{29}$$

$$\mathbf{P}_k^{+} = \left(\mathbf{I}_{6\times6} - \mathbf{K}_k \cdot \mathbf{H}\right)\mathbf{P}_k^{-} \tag{30}$$

Here, the orders of all the matrices are 6×6. Consequently, the computation complexity for the addition, multiplication and

inversion are expensive using the EKF in real-time. Next, the innovation state vector **δx** is calculated from the Kalman gain.

$$\delta\mathbf{x} = \mathbf{K}_k \left(\mathbf{y}_{measured} \otimes \mathbf{y}_{estimated} \right) \quad (31)$$

$$\mathbf{y}_{measured} = \left[\mathbf{q}_e \right]_{measured} \quad (32)$$

$$\mathbf{y}_{estimated} = \left[\mathbf{q}_e \right]_{estimated} \quad (33)$$

where, the $\otimes$ in (31) is the quaternion multiplication. The error quaternion vector $\boldsymbol{\delta q_e}$ is extracted from first three components of the state error vector $\delta\mathbf{x} = \left[\delta\mathbf{q_e}^{\mathrm{T}} \quad \delta(\boldsymbol{\omega}_{\mathrm{bias}} + \boldsymbol{\eta}_{\mathrm{bias}})^{\mathrm{T}} \right]^{\mathrm{T}}$. The error quaternion vector **δq** is used to compensate the propagated satellite quaternion.

$$\delta\mathbf{q} = \left[1 \quad \delta\mathbf{q_e}^{\mathrm{T}} \right]^{\mathbf{T}} \quad (34)$$

$$\mathbf{q}'_{k+1} = \mathbf{q}_{k+1} \otimes \delta\mathbf{q} \quad (35)$$

In addition, the gyro bias is updated as follow: $(\boldsymbol{\omega}_{\mathrm{bias}} + \boldsymbol{\eta}_{\mathrm{bias}})' = (\boldsymbol{\omega}_{\mathrm{bias}} + \boldsymbol{\eta}_{\mathrm{bias}}) + \delta(\boldsymbol{\omega}_{\mathrm{bias}} + \boldsymbol{\eta}_{\mathrm{bias}})$

Then, both state error vectors, $\delta\mathbf{q_e}$ and $\delta(\boldsymbol{\omega}_{\mathrm{bias}} + \boldsymbol{\eta}_{\mathrm{bias}})$ are reset as 3x1 zero vectors. The updated quaternion $\mathbf{q}'_{k+1}$ is then propagated into next available observation time step using the updated $(\boldsymbol{\omega}_{\mathrm{bias}} + \boldsymbol{\eta}_{\mathrm{bias}})'$ and gyro measurement.

B- Gain-scheduled Extended Kalman filter:

To reduce the computational requirement in the conventional EKF method, this section introduces the scheduled Kalman gain algorithm. Equation(29) shows that the Kalman gain computation depends on the matrices **P**, **H,** and **R**. In addition, the matrix **P** depends on both the matrix **Q**, and the satellite rotational speed, **ω**, as shown in (28). Both the matrices **Q** and **R** are constructed from the variance σ^2_n, σ^2_{bias} and σ^2_q. Therefore, the Kalman gain is affected by five factors σ^2_n, σ^2_{bias}, σ^2_q, matrix **H**, and **ω**. The sensor noise variance σ^2_n, σ^2_{bias}, σ^2_q, and matrix **H** are unique for each satellite dynamic system and they have been characterized in section III. Thus, the Kalman gain only depends on the satellite rotational speed, **ω**, which is changing along the orbital path.

When the satellite is operating in space, its attitude profile remains stable in the earth centre inertial frame. There are two main satellite operating modes: nadir pointing and sun pointing as shown in Fig.2. In the sun pointing mode, the satellite solar panel is always perpendicular to the illumination direction to harvest the solar power. In the nadir pointing mode, the bore-sight direction of the camera is always pointing towards the Earth. It is rotating on the orbital plane at 2π/T rad/s where T is the orbital period.

The satellite attitude profile is stable for both operating modes. This means that the Kalman gain is constant for each mode and it can be determined on the ground before launch. Different Kalman gains can then be scheduled for different operating mode. Hence the online Kalman gain computation can be eliminated. The Kalman gain is analytically and explicitly determined based on the satellite dynamic parameters which are variance σ^2_n, σ^2_{bias}, σ^2_q, the matrix **H** and **ω**.

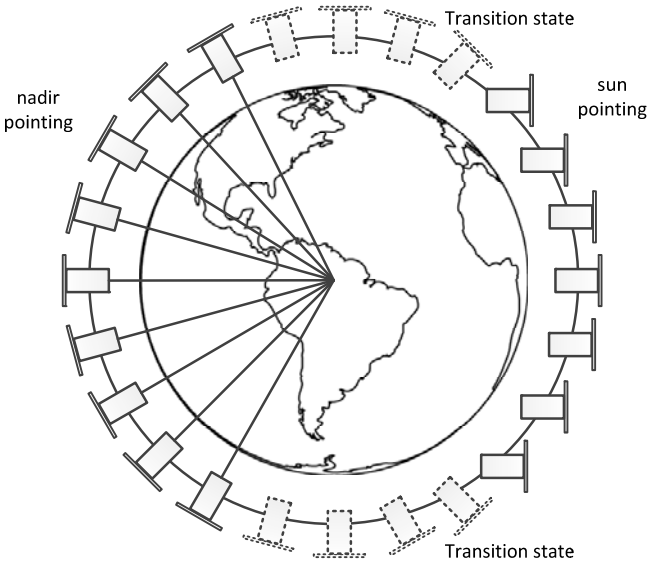

Fig.2: Satellite operation modes

The GSEKF is illustrated in Table I. First, the satellite dynamic parameters are determined based on the sensor calibrations which are shown in section III. In this paper, we are only focusing on two operating modes, which are the sun pointing mode and nadir pointing mode. Therefore, the Kalman gains for sun pointing mode $\mathbf{K}_{np}$, and nadir pointing mode $\mathbf{K}_{sp}$, will be presented in this section. The state vector is propagated using (19). The GSEKF computes the **δx** in a similar fashion as in EKF to compensate for the estimated state error. Finally, the satellite attitude and the gyroscope bias are updated.

Table I: The Gain-Scheduled Extended Kalman Filter

1. Determine system parameters:σ^2_n, σ^2_{bias}, σ^2_q, **H**, **ω.**
2. Load the Kalman gains $\mathbf{K}_{np}$, $\mathbf{K}_{sp}$
3. Propagate the state vector $\mathbf{x}_k$
4. Calculate the innovation state vector $\delta\mathbf{x}_k$
5. Update the propagated satellite attitude and gyroscope bias, then reset $\delta\mathbf{q_e}$ and $\delta(\boldsymbol{\omega}_{\mathrm{bias}} + \boldsymbol{\eta}_{\mathrm{bias}})$ to 3x1 zero vectors.

C- Kalman gain determination method:

This section proposes an analytical method to determine the Kalman gain based on the attitude profile in different operating modes: the sun pointing mode and the nadir pointing mode. Different mode has different attitude profile; hence each of the modes has different Kalman gain.

Sun pointing mode

In the Sun pointing mode, the satellite attitude is stationary, i.e. **ω** = **0**. Substitute this into (16) and the state transition matrix **Φ** becomes an identity matrix.

$$\boldsymbol{\Phi} = \mathbf{I}_{6\times 6} \quad (36)$$

Under this condition, the state error covariance, $\mathbf{P}^-_k$, in (28) can be reduced as

$$\mathbf{P}^-_k = \mathbf{P}^+_{k-1} + \mathbf{Q} \quad (37)$$

The Kalman gain, $\mathbf{K}_k$, and matrix, $\mathbf{P}^+_k$, in (29)and (30) become

$$\mathbf{K}_k = \mathbf{P}_k^- \left(\mathbf{P}_k^- + \mathbf{R}\right)^{-1} \quad (38)$$

$$\mathbf{P}_k^+ = \left(\mathbf{I}_{6\times 6} - \mathbf{K}_k\right)\mathbf{P}_k^- \quad (39)$$

Substitutes (37) into(38):

$$\mathbf{K}_k = \left(\mathbf{P}_{k-1}^+ + \mathbf{Q}\right)\left(\mathbf{P}_{k-1}^+ + \mathbf{Q} + \mathbf{R}\right)^{-1} \quad (40)$$

Substitute (37) and (40) into(39):

$$\mathbf{P}_k^+ = \left(\mathbf{I}_{6\times 6} - \left(\mathbf{P}_{k-1}^+ + \mathbf{Q}\right)\left(\mathbf{P}_{k-1}^+ + \mathbf{Q} + \mathbf{R}\right)^{-1}\right)\left(\mathbf{P}_{k-1}^+ + \mathbf{Q}\right) \quad (41)$$

Assuming that Δt is small enough, $\mathbf{P} \equiv \mathbf{P}^+_k = \mathbf{P}^+_{k-1}$. Equation (41) is solved in term of matrix **P**:

$$\mathbf{PP} + \mathbf{PQ} - \mathbf{QR} = \mathbf{0} \quad (42)$$

Because the matrices **Q** and **R** are diagonal, the solution for the matrix **P** is:

$$\mathbf{P} = \frac{\sqrt{\mathbf{Q}^2 + 4\mathbf{QR}} - \mathbf{Q}}{2} \quad (43)$$

The Kalman gain matrix, $\mathbf{K}_{sp}$, can be found by substituting (43) into(40) as

$$\mathbf{K}_{sp} = \left(\sqrt{\mathbf{Q}^2 + 4\mathbf{QR}} + \mathbf{Q}\right)\left(\sqrt{\mathbf{Q}^2 + 4\mathbf{QR}} + \mathbf{Q} + 2\mathbf{R}\right)^{-1} \quad (44)$$

Nadir pointing mode

In the nadir pointing mode, the satellite rotational speed, **ω**, is 2π/T rad/s, where T is the satellite orbital period. The matrix **Φ** is given as.

$$\mathbf{\Phi} = \mathbf{I}_{6\times 6} + \mathbf{F}\Delta t \quad (45)$$

Under this condition, the matrix $\mathbf{P}^-_k$ is same as(37). The Kalman gain, $\mathbf{K}_k$, and matrix $\mathbf{P}^+_k$ are the same as (38) and (39) respectively. By substituting (28) into(38), we obtain

$$\mathbf{K}_k = \left(\mathbf{\Phi}\cdot\mathbf{P}_{k-1}^+\cdot\mathbf{\Phi}^{\mathbf{T}} + \mathbf{Q}\right)\left(\mathbf{\Phi}\cdot\mathbf{P}_{k-1}^+\cdot\mathbf{\Phi}^{\mathbf{T}} + \mathbf{Q} + \mathbf{R}\right)^{-1} \quad (46)$$

Then, substitute (28) and (46) into (39):

$$\mathbf{P}_k^+ = \left(\mathbf{I}_{6\times 6} - \left(\mathbf{\Phi}\cdot\mathbf{P}_{k-1}^+\cdot\mathbf{\Phi}^{\mathbf{T}} + \mathbf{Q}\right)\left(\mathbf{\Phi}\cdot\mathbf{P}_{k-1}^+\cdot\mathbf{\Phi}^{\mathbf{T}} + \mathbf{Q} + \mathbf{R}\right)^{-1}\right)\left(\mathbf{\Phi}\cdot\mathbf{P}_{k-1}^+\cdot\mathbf{\Phi}^{\mathbf{T}} + \mathbf{Q}\right) \quad (47)$$

Assuming that Δt is small enough, which is $\mathbf{P} \equiv \mathbf{P}^+_k = \mathbf{P}^+_{k-1}$. Furthermore, it can be assumed that **ω** is small enough, that Φ is closed to a diagonal matrix. Therefore, by solving equation (47) for matrix **P**, we obtain:

$$\mathbf{\Phi}^2\mathbf{P}^2 + \left(\mathbf{Q} - \mathbf{R}\left(\mathbf{\Phi}^2 - \mathbf{I}_{6\times 6}\right)\right)\mathbf{P} - \mathbf{QR} \approx \mathbf{0} \quad (48)$$

Similar to sun pointing mode, the matrix **P** can be solved as:

$$\mathbf{P} = \frac{\sqrt{\left(\mathbf{Q} - \mathbf{R}\left(\mathbf{\Phi}^2 - \mathbf{I}_{6\times 6}\right)\right)^2 + 4\mathbf{\Phi}^2\mathbf{QR}} - \left(\mathbf{Q} - \mathbf{R}\left(\mathbf{\Phi}^2 - \mathbf{I}_{6\times 6}\right)\right)}{2\mathbf{\Phi}^2} \quad (49)$$

The Kalman gain matrix, $\mathbf{K}_{np}$, can be obtained by substituting (49) into(46) to yield the following

$$\mathbf{K}_{np} = \left(\frac{\sqrt{\left(\mathbf{Q} - \mathbf{R}\left(\mathbf{\Phi}^2 - \mathbf{I}_{6\times 6}\right)\right)^2 + 4\mathbf{\Phi}^2\mathbf{QR}} - \left(\mathbf{Q} - \mathbf{R}\left(\mathbf{\Phi}^2 - \mathbf{I}_{6\times 6}\right)\right)}{2} + \mathbf{Q}\right) \left(\frac{\sqrt{\left(\mathbf{Q} - \mathbf{R}\left(\mathbf{\Phi}^2 - \mathbf{I}_{6\times 6}\right)\right)^2 + 4\mathbf{\Phi}^2\mathbf{QR}} - \left(\mathbf{Q} - \mathbf{R}\left(\mathbf{\Phi}^2 - \mathbf{I}_{6\times 6}\right)\right)}{2} + \mathbf{Q} + \mathbf{R}\right)^{-1} \quad (50)$$

After the scheduled Kalman gains in (44) and (50)are calculated, they are stored on the satellite memory. Then, the GSEKF load the Kalman gain with respect to its operating mode, and estimates the satellite attitude using the algorithm presented in Table I.

V. SIMULATION & EXPERIMENTAL RESULTS

Simulation and experiment have been conducted to evaluate the GSEKF performance. The software-in-loop (SIL) simulation has been developed to simulate the satellite dynamics in space. The GSEKF is compared with the EKF in terms of the Kalman gain, computation complexity and attitude accuracy. To evaluate the stability of GSEKF, the Fisher information matrix is derived. For the experimental study, the setup includes a sun simulator, a Helmholtz cage and a two axes rate table to simulate the dynamic motion in space.

A- Simulation setup

The software-in-loop SIL simulates the satellite orbital motion, space environment, satellite dynamics and the attitude sensors. The SIL simulator calculates the satellite orbital motion using SGP4 model with the input satellite orbital parameters (i.e. TLE). The space environment simulates the Earth magnetic field, and the sun illumination in space. The Earth magnetic field and the sun illumination are calculated based on the IGRF-11 model, and the sun vector model. The satellite dynamics determine the satellite rotational speed, and the satellite attitude from the exerted torques. The attitude sensors (gyroscope, sun sensor and magnetometer) simulate the real-time readings from the satellite dynamics.

Table II: The SIL simulator parameters

Orbit propagator model	SGP4
Orbit parameters (TLE)	
• Inclination	1.7228 radian
• RAAN	3.3253 radian
• Eccentricity	9.2990e-004
• Argument perigee	3.1796 radian
• Mean anomaly	3.1056 radian
• Mean motion	0.0620 radian/minute
Magnetic field model	IGRF-11 13th order
Simulation start time	[2012-07-02-00-14-23]
Satellite orbital period	101 minutes
Satellite moment inertia	$\begin{bmatrix} 3.7507 & 0.0133 & 0.0031 \\ 0.0133 & 4.6763 & 0.0486 \\ 0.0030 & 0.0486 & 1.6244 \end{bmatrix} 10^{-2}$
Initial attitude $\mathbf{q}_0$	[0.1522 -0.3244 -0.6786 -0.6411]
Initial speed $\boldsymbol{\omega}_0$	[2 , 2, 2] degree/second
Disturbance torque	Solar radiation Aerodynamic drag Gravity disturbance
Gyroscope noise variance σ^2_n	0-2 $(\text{deg/s})^2$
Measurement noise variance σ^2_q	0-2$(\text{deg})^2$
Satellite operation mode	Nadir pointing and sun pointing

The EKF and GSEKF algorithms presented in section IV have been integrated into the SIL simulator to acquire the gyroscope, sun sensor, and magnetometer measurements. The satellite attitude is estimated at the frequency of 10Hz. In addition, the GSEKF uses the gyroscope noise variance, σ^2_n, and the measured quaternion variance, σ^2_q, which are characterized in section III to compute the scheduled Kalman gain offline. The initial parameters of the SIL simulator are summarized in Table II. The nano-satellite orbital period is assumed to be 101 minutes in the polar orbit.

B- Kalman gain comparison

The two SIL simulations have been executed: EKF and GSEKF simulation. Each simulation is run for one satellite orbit period. The Kalman gains in the EKF and GSEKF are recorded during the simulations. Fig.3 compares the scheduled Kalman gain and the conventional Kalman filter gain in the sun pointing mode with varying matrix **Q**. Fig.4 compares the scheduled Kalman gain and the conventional Kalman filter gain in the sun pointing mode with varying matrix **R**. The conventional Kalman filter gain converges to the steady state after 5ms. On the other hand, the scheduled Kalman gain is directly calculated from the process noise and measurement noise variances using(44). Both figures show that the scheduled Kalman gain matches the conventional Kalman filter gain value in both the sun pointing mode and the nadir pointing mode.

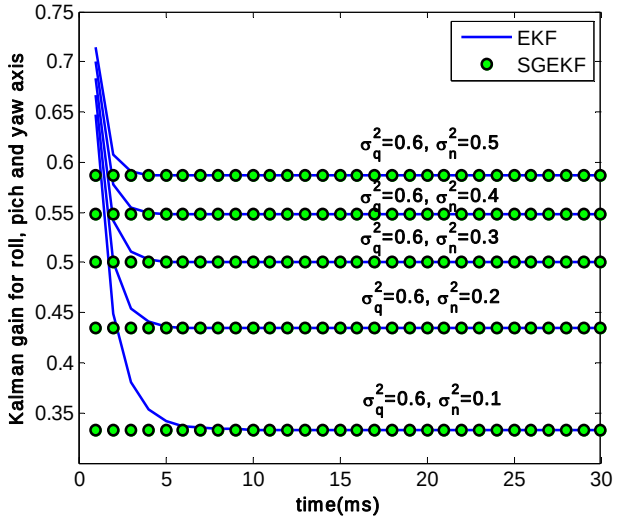

Fig.3: Kalman gain in the sun pointing mode with varying Q (σ^2_q=0.6(deg)^2, σ^2_n=0.1-0.5(deg/s)^2)

To study the effect of noise variance on the proposed GSEKF, an extensive simulation study is conducted. In this study, there are 25 SIL simulations for each combination of measurement and process noise covariance. Fig. 5 shows the relationships between the scheduled Kalman gain, the process noise and measurement noise variance. From Fig. 5, it is observed that when the process noise variance increases from 0.1 to 0.5, the Kalman gain increases from 0.32 to 0.57. When the measurement noise variance increases from 0.1 to 0.5, the Kalman gain decreases from 0.87 to 0.65. When the process noise increases, the gyroscope signal has larger noise variance. Hence the propagated attitude error in (19) is increased. It required higher Kalman gain to compensate for the error. When the measurement noise variance increases, the sun sensor and magnetometer signals have larger noise variance. Hence, a lower Kalman gain is required to reduce the external noise effect on the system. In conclusion, the GSEKF calculates the optimal Kalman gain to compensate for the internal process noise and external measurement noise.

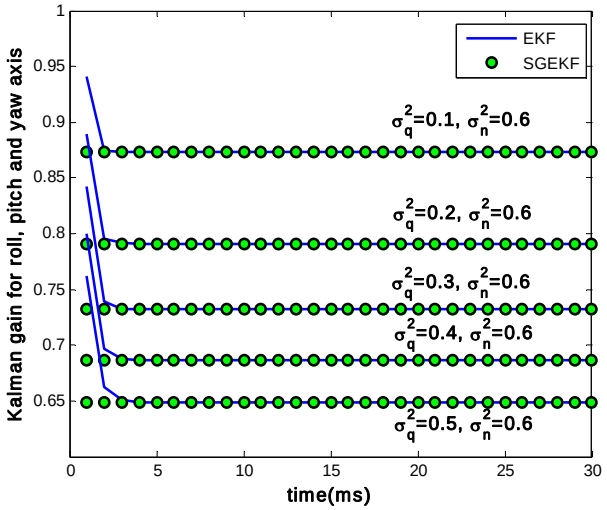

Fig.4: Kalman gain in the sun pointing mode with varying R (σ^2_q=0.1-0.5(deg)^2, σ^2_n=0.6(deg/s)^2)

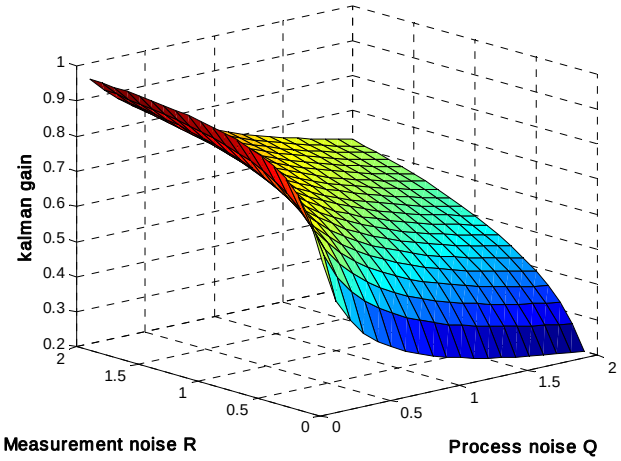

Fig.5: Kalman gain in sun pointing mode(σ^2_q=0-2(deg/s)^2, σ^2_n=0-2(deg/s)^2)

C- Computational complexity comparison:

Table III compares the computational complexity of MEKF, Murrell's version and GSEKF algorithms in terms of the number of multiplication. The GSEKF algorithm consists of the state propagation and update processes. Its computational complexity is $3n^2$, where n is the dimension of state vector. The MEKF algorithm consists of the state propagation, Kalman update, state error covariance update, and Kalman gain computation. Its computational complexity is $(19n^3 + 9n^2 - n)/3$. Table III shows that the Kalman gain calculation has a

higher complexity order ($O(n^3)$) than the state propagation and Kalman update($O(n^2)$). This implies that the Kalman gain computation requires a significant processing time. The Kalman gain and state error covariance computation are not required in the GSEKF, leading to a significant reduction in processing time. The Murrell version has significantly reduced the Kalman gain computation from third order into first order. Its total complexity is (12n3 + 9n2+116n)/3. The GSEKF still has a lower complexity than the Murrell version, because the GSEKF does not require Kalman gain computation.

Fig.6 shows the MEKF, Murrell's version and GSEKF algorithm complexity with respect to the state vector dimension *n*. The processing time for the EKF is exponentially increased with *n*. In the case of *n*=6, the MEKF requires 1474 multiplications and the Murrell version requires 1024 multiplications while the GSEKF requires only 108 multiplications. Thus the processing time is reduced by 86.29% and 89.45%. If the dimension of state vector is larger, the GSEKF will have greater reduction in processing time as compared to the EKF.

Table III: EKF and GSEKF algorithm complexity

	EKF	**Murrell's version**	**GSEKF**
$\mathbf{\Phi} = \mathbf{I}_{6\times6} + \mathbf{F}\Delta t$	n^2	n^2	n^2
$\mathbf{x}_k = \mathbf{\Phi}\mathbf{x}_{k-1} + \mathbf{G}\mathbf{w}_{k-1}$	n^2	n^2	n^2
$\mathbf{P}_k^- = \mathbf{\Phi}_k \cdot \mathbf{P}_{k-1}^+ \cdot \mathbf{\Phi}_k^T + \mathbf{Q}$	$2n^3$	$2n^3$	0
$\mathbf{K}_k = \mathbf{P}_k^- \cdot \mathbf{H}^T \cdot \left(\mathbf{H} \cdot \mathbf{P}_k^- \cdot \mathbf{H}^T + \mathbf{R}\right)^{-1}$	$(13n^3 - n)/3$	$(116n)/3$	0
$\mathbf{P}_k^+ = \left(\mathbf{I}_{6\times6} - \mathbf{K}_k \cdot \mathbf{H}\right)\mathbf{P}_k^-$	$2n^3$	$2n^3$	0
$\delta\mathbf{x}_k = \mathbf{K}\delta\mathbf{y}_k$	n^2	n^2	n^2
Total	$(19n^3 + 9n^2 - n)/3$	$(12n^3+9n^2+116n)/3$	$3n^2$

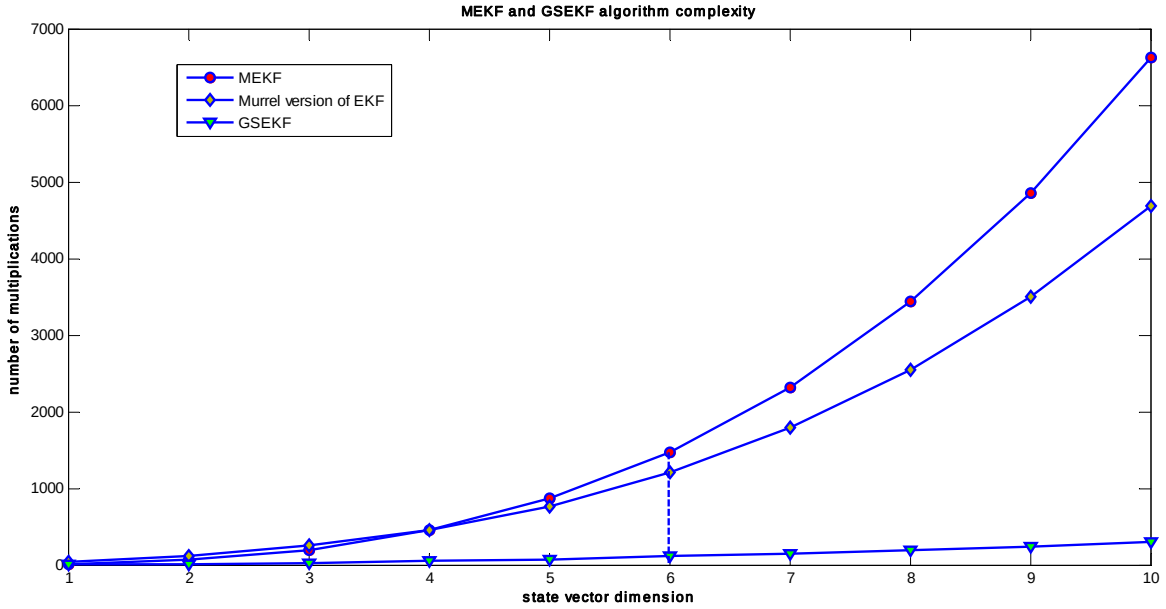

Fig.6: EKF and GSEKF algorithm complexity

D- Stability analysis

The stability analysis of GSEKF is studied based on its state error covariance, **P**. Let the state error be defined as $\tilde{\mathbf{x}} = \mathbf{x} - \hat{\mathbf{x}}$, where $\mathbf{x}$ is the true state vector, and $\hat{\mathbf{x}}$ is the estimated state vector **P** matrix corresponds to:

$$\mathbf{P} = \{\tilde{\mathbf{x}}\tilde{\mathbf{x}}^T\} \geq \Gamma^{-1} \tag{50}$$

Where the matrix **Γ** is the Fisher information matrix defined as

$$\Gamma \equiv -E\left\{\frac{\partial}{\partial\tilde{\mathbf{x}}\tilde{\mathbf{x}}^T}\mathbf{J}(\mathbf{x})\right\} \tag{50}$$

By considering the cost function of Kalman Filter [36]

corresponds to:

$$\mathbf{J(x)}=\frac{1}{2}(\mathbf{\Phi x}-\mathbf{\Phi\hat{x}})^{\mathrm{T}}\mathbf{Q}^{-1}(\mathbf{\Phi x}-\mathbf{\Phi\hat{x}})+\frac{1}{2}(\mathbf{Hx}-\mathbf{H\hat{x}})^{\mathrm{T}}\mathbf{R}^{-1}(\mathbf{Hx}-\mathbf{H\hat{x}}) \quad (51)$$

The Fisher information matrix can be determined by following the procedure in[37], which results

$$\Gamma=\mathbf{\Phi}^{\mathrm{T}}\mathbf{Q}^{-1}\mathbf{\Phi}+\mathbf{H}^{\mathrm{T}}\mathbf{R}^{-1}\mathbf{H} \quad (51)$$

To ensure stability of the GSEKF, the matrix F shall not exhibit singularity, i.e. its determinant does not approach zero, at any satellite rotational speed. The SIL simulator is employed to evaluate the system stability during the transition state, from the nadir pointing mode to the sun tracking mode, and back to nadir pointing mode. The transition state is simulated by varying the rotational speed from -10 to 10 degrees per second.

Fig. 7 presents the change of Fisher information matrix determinant with respect to the rotational speed. The result shows that the matrix determinant does not approach zero at all time. Therefore, it can be concluded that the GSEKF does not suffer the instability during the transition either from nadir pointing mode to sun point mode, or from sun pointing mode to nadir pointing mode. The Fisher information matrix determinant has small variation (< 10^{-5}) because of the small variation in rotation speed.

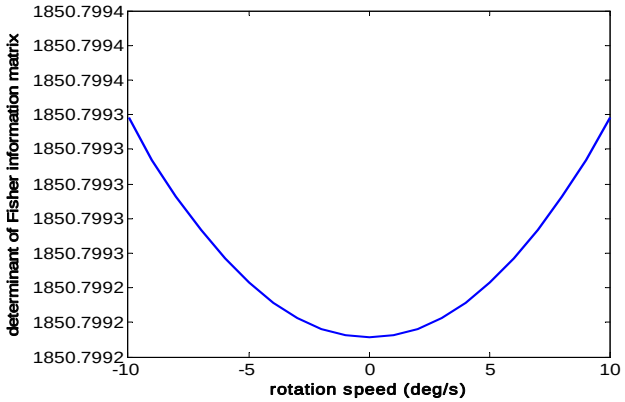

Fig.7: Fisher information matrix

E- Simulation Results – Attitude Accuracy Comparison:

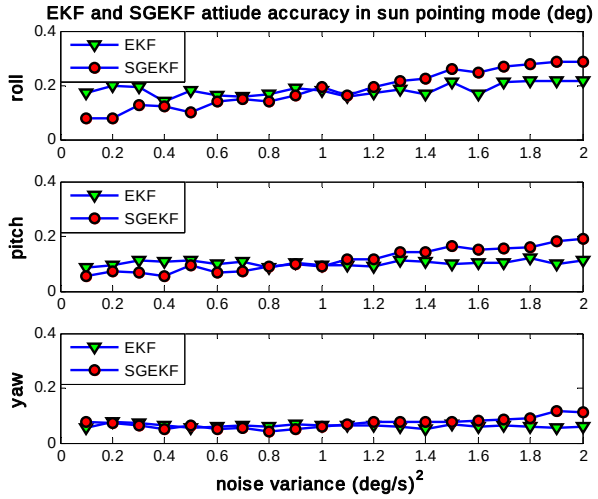

Fig.8: EKF and GSEKF attitude accuracy in sun pointing mode

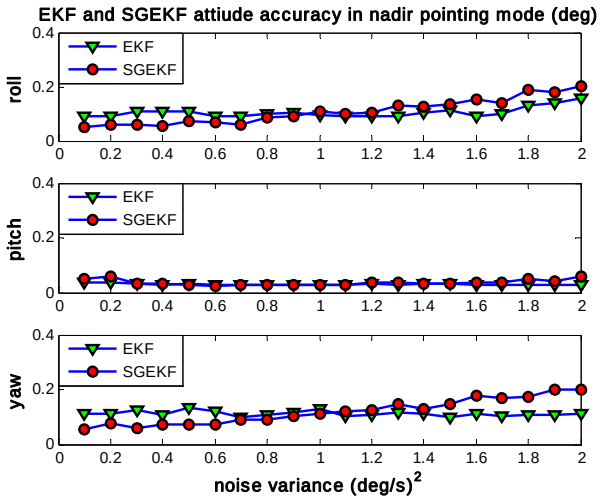

Fig.9: EKF and GSEKF attitude accuracy in nadir pointing mode

Fig.8 and 9 compare the estimated attitude accuracy between the GSEKF and EKF with respect to different noise variance in both the sun pointing mode and the nadir pointing mode. The process noise and the measurement noise covariance are considered to be equal in this simulation,$\sigma^2_q = \sigma^2_n$. The noise variance ranges from 0 to 2(deg/s)^2. The attitude accuracy is compared in terms of the roll, pitch, and yaw angles. The results show that the attitude accuracy falls within 0 to 0.2 degrees during the entire orbital period. The GSEKF error is higher than the EKF when the noise variance is higher. Both operation modes show that the GSEKF has a lower attitude estimation error than the EKF when the noise variance is lower than 1 degree.

F- Experimental setup and Result

The experimental setup of the attitude determination system is shown in Fig.10. It consists of a Helmholtz magnetic cage, a sun simulator and a nano-satellite prototype. The Helmholtz magnetic cage is capable of producing a homogeneous magnetic field in any desired magnitude and direction. It consists of three orthogonal coil pairs. The desired magnetic field can be generated by providing a suitable coil current. The sun simulator is an optical instrument that simulates the sunlight illumination as shown in Fig.11. The light source is closely matched with the solar spectrum with a solar power output of 1300 W/m^2. The sun simulator uses mirrors to direct the light beam from the arc lamp source to the target plane, and produces high intensity, uniform illumination at the target plane. The sun simulator is placed in front of the nano-satellite sun sensor.

The nano-satellite prototype has as attitude determination system board. It has two sun sensors placed on the -Z direction, a three-axis magnetometer and a gyroscope. The sun sensor is used to measure the sun vector from the sun simulator. The magnetometer measures the generated magnetic field from the Helmholtz cage. The nano-satellite is fixed on a rotational stage that allows the nano-satellite to be rotated about one axis at ±30 arcsec accuracy. Its rotation is simulated in the nadir

pointing mode. The rotational speed is 2π/T rad/s where T is the satellite orbital period. The nano-satellite is only rotated from -30 to 30 degrees due to the fact that the sun sensor only has 60 degrees field of view. The satellite attitude is computed by the GSEKF algorithm and compared with the true satellite attitude.

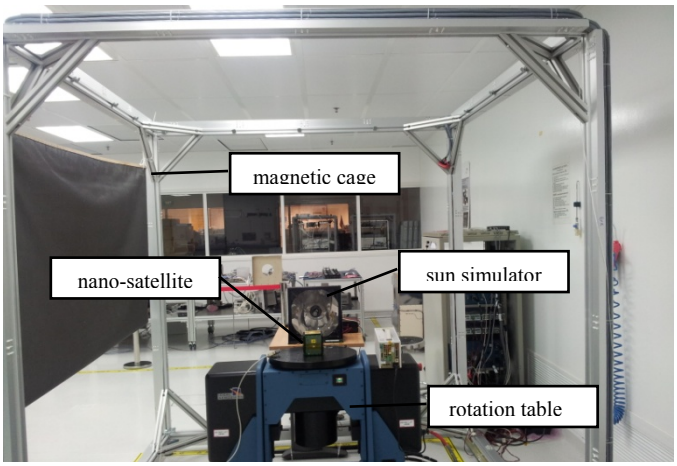

Fig.10: Experiment setup

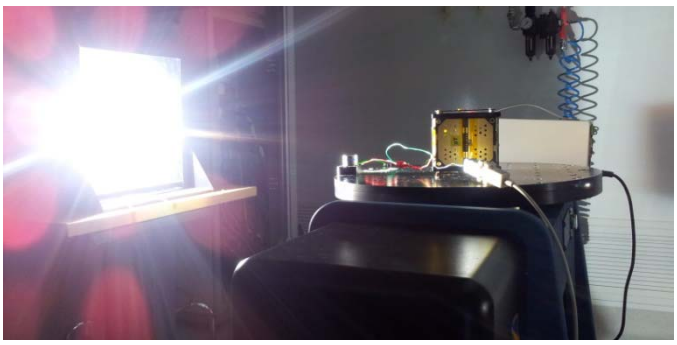

Fig.11: Sun simulator

Fig.12 compares the estimated attitude using the GSEKF and the truth attitude in the yaw axis. The satellite is rotated about the yaw axis at 2π/T rad/s, which is sampled at a frequency of 10Hz.The result shows that the GSEKF generates accurate satellite attitude.

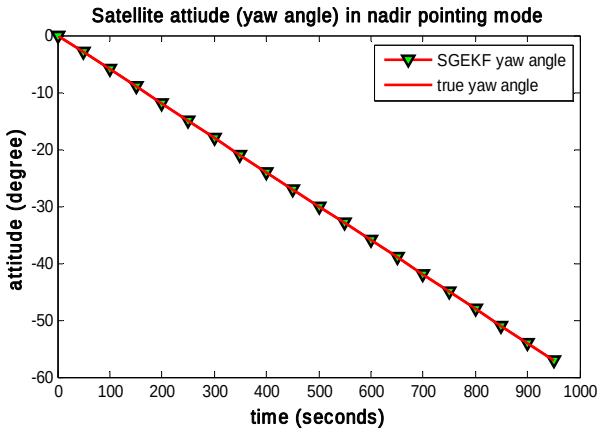

Fig.12: Satellite attitude in nadir pointing mode

VI. CONCLUSIONS

This paper presented a scheduled gain extended Kalman filter algorithm for the attitude determination of a nano-satellite. Two scheduled Kalman gain for two satellite operating modes namely the sun pointing mode and the nadir pointing mode have been presented. The proposed method computes the scheduled Kalman gain offline based on the sensors' noise variance, the measured quaternion variance, the observation matrix, and the satellite rotational speed. The simulation results show that the scheduled Kalman gain matches the conventional Kalman gain. Furthermore, the experimental result has confirmed that the proposed GSEKF is applicable in the nano-satellite attitude determination system. The key advantage of the proposed GSEKF algorithm is the much lower computational complexity than the MEKF and Murrell's version, and the processing time could be reduced by 86.29% and 89.45%. Moreover, the result shows that the GSEKF has comparable attitude estimation accuracy to the EKF.

REFERENCES

[1] Y. Oshman and F. L. Markley, "Spacecraft attitude/rate estimation using vector-aided GPS observations," *Aerospace and Electronic Systems, IEEE Transactions on,* vol. 35, pp. 1019-1032, 1999.

[2] A. Gelb, *Applied Optimal Estimation*: MIT Press, 1974.

[3] R. G. Brown and P. Y. C. Hwang, *Introduction to Random Signal and Applied Kalman Filtering*. New York: Wiley, 1994.

[4] E. J. Lefferts, F. L. Markley, and M. D. Shuster, "Kalman Filtering for spacecraft attitude determination," *Journal of Guidance, Control and Dynamics,* vol. 5, pp. 417-429, 1982.

[5] F. L. Markley, "Attitude error representations for Kalman filtering " *Journal of Guidance, Control and Dynamics,* vol. 26, pp. 311-317, 2003.

[6] J. L. Crassidis, F. L. Markley, and Y. Cheng, "A Survey of Nonlinear Attitude Estimation Methods," *Journal of Guidance, Control, and Dynamics,* vol. 30, pp. 12-28, 2007.

[7] I. Y. Bar-Itzhack and Y. Oshman, "Attitude Determination from Vector Observations: Quaternion Estimation," *Aerospace and Electronic Systems, IEEE Transactions on,* vol. AES-21, pp. 128-136, 1985.

[8] T. Bak, "Onboard attitude determination for a small satellite," presented at the Third Internationl Conference on Spacecraft Guidance, Navigation and Control Systems, Noordwijk, The Netherlands, 1996.

[9] J. L. Crassidis and J. L. Junkins, *Optimal Estimation of Dynamics System*: CRC Press, 2011.

[10] I. Y. Bar-Itzhack, J. Deutschmann, and F. L. Markley, "Quaternion Normalization in Addtive EKF for Spacecraft Attitude Determination," presented at the AIAA Guidance, navigation and Control Conference, New Orleans, LA, 1991.

[11] D. Choukroun, I. Y. Bar-Itzhack, and Y. Oshman, "Novel quaternion Kalman filter," *Aerospace and Electronic Systems, IEEE Transactions on,* vol. 42, pp. 174-190, 2006.

[12] J. L. Crassidis, "Sigma-point Kalman filtering for integrated GPS and inertial navigation," *Aerospace and*

Electronic Systems, IEEE Transactions on, vol. 42, pp. 750-756, 2006.
[13] M. Abdelrahman and P. Sang-Young, "Sigma-Point Kalman Filtering for Spacecraft Attitude and Rate Estimation using Magnetometer Measurements," *Aerospace and Electronic Systems, IEEE Transactions on,* vol. 47, pp. 1401-1415, 2011.
[14] A. Giannitrapani, N. Ceccarelli, F. Scortecci, and A. Garulli, "Comparison of EKF and UKF for Spacecraft Localization via Angle Measurements," *Aerospace and Electronic Systems, IEEE Transactions on,* vol. 47, pp. 75-84, 2011.
[15] D. Choukroun, H. Weiss, I. Y. Bar-Itzhack, and Y. Oshman, "Quaternion Estimation from Vector Observations using a Matrix Kalman Filter," *Aerospace and Electronic Systems, IEEE Transactions on,* vol. 48, pp. 3133-3158, 2012.
[16] K. Xiong, T. Liang, and L. Yongjun, "Multiple model Kalman filter for attitude determination of precision pointing spacecraft," *Acta Astronautica,* vol. 68, pp. 843-852, 2011.
[17] X. Tang, Z. Liu, and J. Zhang, "Square-root quaternion cubature Kalman filtering for spacecraft attitude estimation," *Acta Astronautica,* vol. 76, pp. 84-94, 2012.
[18] E. Koyuncu, E. Baskaya, M. Cihan, S. Isiksal, M. Fidanoglu, C. Akay*, et al.*, "ITU-pSAT II: High-precision nanosatellite ADCS development project," in *Recent Advances in Space Technologies (RAST), 2011 5th International Conference on*, 2011, pp. 500-505.
[19] A. A. M. P. Keui, M. Fadly, O. Sidek, and M. A. M. Said, "EKF implementation on S3CEV40 for InnoSAT attitude determination system," in *Computer Applications and Industrial Electronics (ICCAIE), 2011 IEEE International Conference on*, 2011, pp. 373-378.
[20] G. Falbel and M. A. Paluszek, "An ultra low weight/low cost three axis attitude readout system for nano-satellites," in *Aerospace Conference, 2001, IEEE Proceedings.*, 2001, pp. 2469-2481 vol.5.
[21] G. F. de Oliveira, J. Y. Ishihara, R. A. Borges, H. C. Ferreira, A. M. Kulabukhov, V. A. Larin*, et al.*, "A Low-Cost Attitude Determination and Control System for the UYS-1 nanosatellite," in *Aerospace Conference, 2013 IEEE*, 2013, pp. 1-14.
[22] W. Blackwell, G. Allen, C. Galbraith, T. Hancock, R. Leslie, I. Osaretin*, et al.*, "Nanosatellites for earth environmental monitoring: The MicroMAS project," in *Geoscience and Remote Sensing Symposium (IGARSS), 2012 IEEE International*, 2012, pp. 206-209.
[23] B. Russell, L. Clement, J. Hernandez, A. Byagowi, D. Schor, and W. Kinsner, "Implementation of a nanosatellite attitude determination and control system for the T-Sat1 mission," in *Electrical and Computer Engineering (CCECE), 2013 26th Annual IEEE Canadian Conference on*, 2013, pp. 1-5.
[24] J. C. Springmann, A. J. Sloboda, A. T. Klesh, M. W. Bennett, and J. W. Cutler, "The attitude determination system of the RAX satellite," *Acta Astronautica,* vol. 75, pp. 120-135, 2012.
[25] T. Kobayashi, D. L. Simon, and J. S. Litt, "Application of a constant gain extended kalman filter for in-flight estimation of aircraft engine performance parameters," NASA 2005.
[26] J. Chang, G. N. Taranto, and J. H. Chow, "Dynamic state estimation in power system using a gain-scheduled nonlinear observer," in *Control Applications, Proceedings of the 4th IEEE Conference on*, 1995, pp. 221-226.
[27] T. Fossen and J. P. Strand, "Passive nonlinear observer design for ships using lyapunov methods: full-scale experiments with a supply vessel," *Automatica,* vol. 35, pp. 3-16, 1999.
[28] D. P. Horkheimer, "Gain scheduling of an Extended Kalman Filter for use in an attitude/heading estimation system," University of Minnesota, 2012.
[29] J. Lenz and A. S. Edelstein, "Magnetic sensors and their applications," *IEEE Sensors J.,* vol. 6, pp. 631-649, 2006.
[30] J. R. Wertz, "Attitude hardware," in *Spacecraft attitude determination and control*, ed: Computer Sciences Corporation, 1978 pp. 180-184.
[31] J. R. Wertz, *Spacecraft attitude determination and control*: Computer Sciences Corporation, 1978.
[32] H. Curtis, *Orbital Mechanics: For Engineering Students* 2ed.: Butterworth-Heinemann, 2005
[33] C. C. Finlay, S. Maus, C. D. Beggan, T. N. Bondar, A. Chambodut, T. A. Chernova*, et al.*, "International geomagnetic reference field: the eleventh generation," *Geophysical J. International,* vol. 183, pp. 1216-1230, 2010.
[34] D. Gebre-Egziabher, R. C. Hayward, and J. D. Powell, "Design of multi-sensor attitude determination systems," *Aerospace and Electronic Systems, IEEE Transactions on,* vol. 40, pp. 627-649, 2004.
[35] H. Black, "A Passive System for Determining the Attitude of a Satellite," *AIAA Journal,* vol. 2, pp. 1350-1351, 1964.
[36] Y. Gu and D. S. Oliver, "Then Ensemble Kalman Filter for Continuous Updating of Reservoir Simulation Models," *Jounral of Energy Resources Technology,* vol. 128, pp. 79-81, 2006.
[37] M. S. Andrle, J. L. Crassidis, R. Linares, Y. Cheng, and B. Hyun, "Deterministic Relative Attitude Determination of Three-Vehicle Formations," *Journal of Guidance, Control, and Dynamics,* vol. 32, pp. 1077-1088, 2009

Minh Duc Pham received the B.Eng. and M.E degree in Electrical and Electronic Engineering from Nanyang Technological University, Singapore in 2010 and 2012 respectively. His research interests include satellite attitude determination, Kalman filter, star sensor, image processing and embedded system.

Kay-Soon Low (M'88-SM'00) received the B.Eng. degree in Electrical Engineering from the National University of Singapore, Singapore, and the Ph.D. degree in Electrical Engineering from the University of New South Wales, Sydney, Australia.

He has worked in the academia as well as in the industry. He joined the School of Electrical and Electronic Engineering, Nanyang Technological University in 1994 first as a lecturer and subsequently became an Associate Professor. He has successfully supervised 42 graduate theses and delivered 43 funded projects. He has served as consultants to many companies and has 19 patents on nonlinear circuits, UWB systems and imaging sensor. His present funded projects are in the field of wireless sensor network, solar energy and satellite system. He has been the centre director of Satellite Research Centre (SaRC), Nanyang Technological University since April 2009. The centre has successfully developed four satellites (X-SAT, VELOX-PII, VELOX-PIII and VELOX-I). All have been successfully launched between April 2011 and June 2014. In orbit experiments have been successfully demonstrated. Dr Low has been a senior member of IEEE since 2000.

Shu Ting Goh is currently a research fellow in Satellite Research Centre, School of Electrical and Electronic Engineering, Nanyang Technological University. He received his Ph.D. degree at the Mechanical Engineering - Engineering Mechanics Department, Michigan Technological University in 2012. His research interests include the parameter optimization, data assimilation, attitude determination, and Kalman filter implementation on photovoltaic module characteristic identification, battery state of charge estimation, acoustic tracking and localization, satellite attitude and position estimation and object tracking.

Shoushun Chen (M'05) received his B.S. degree from Peking University, M.E. degree from Chinese Academy of Sciences and PhD degree from Hong Kong University of Science and Technology in 2000, 2003 and 2007, respectively.

He held a post-doctoral research fellowship in the Department of Electronic and Computer Engineering, Hong Kong University of Science and Technology for one year after graduation. From February 2008 to May 2009 he was a post-doctoral research associate within the Department of Electrical Engineering, Yale University. In July 2009, he joined Nanyang Technological University as an assistant professor.

Dr. Chen is a senior member of IEEE. He serves as a technical committee member of Sensory Systems, IEEE Circuits and Systems Society (CASS); Associate Editor of IEEE Sensors Journal; Program Director (Smart Sensors) of VIRTUS, IC Design Centre of Excellence, NTU. His research interests include smart vision sensors, motion detection sensors, energy-efficient algorithms for bio-inspired vision, and analog/mixed-signal VLSI circuits and system